Robust Incremental Nonlinear Dynamic Inversion Control Using Angular Accelerometer Feedback

Çakiroğlu, Can; van Kampen, Erik-Jan; Chu, Qiping

DOI
10.2514/6.2018-1128

Publication date
2018

Document Version
Accepted author manuscript

Published in
Proceedings of the 2018 AIAA Information Systems-AIAA Infotech @ Aerospace

Robust Incremental Nonlinear Dynamic Inversion Control Using Angular Accelerometer Feedback

Can Cakiroglu*, Erik-Jan van Kampen†, Qiping Chu‡
Control and Simulation, Department Control and Operations
Delft University of Technology, Delft, The Netherlands

Incremental Nonlinear Dynamic Inversion (INDI) is a robust nonlinear control technique that is an adaptation of nonlinear dynamic inversion (NDI). By assuming time scale separation between fast and slow dynamics, and by using angular acceleration feedback, the inner loop of INDI directly controls angular accelerations with incremental control effector inputs. In practice, most applications rely on derivation and filtering of angular rates to obtain angular accelerations. The added steps in the feedback loop introduce transport delays and thereby reduce the tracking performance of the controller. Recent technological advancements in angular accelerometer design have made it feasible to use angular accelerometers for direct sensing of the accelerations. Simulations are done using a CS-25 type aircraft model in combination with real-world sensor characteristics and turbulence. The main contribution of this paper is the effects of using angular accelerometers in INDI control. Controller performance in the investigated configuration of angular accelerometers, rate gyros and effector deflection sensors is limited by the high transport delays of the gyros. Using the angular accelerometer signals to obtain the rates, controller tracking performance is improved whilst requiring lower actuator effort. Further contributions are a study on angular accelerometer misalignment showing that INDI control rejects sensor misalignment successfully, and finally a study on the effects of using uncalibrated control effector deflection feedback showing the high sensitivity of INDI control to uncalibrated effector sensors.

Nomenclature

$\bar{c}$	Mean aerodynamic chord, m
C_l, C_m, C_n	Dimensionless rolling, pitching and yawing moment coefficients
$\underline{f}$	Generic vector function
G	Control effectiveness matrix
$\underline{h}$	Generic vector function
I	Mass moment of inertia tensor
L, M, N	Rolling, pitching and yawing moments, Nm
p, q, r	Roll, pitch and yaw rates in the body frame, rad/s
$\dot{p}, \dot{q}, \dot{r}$	Roll, pitch and yaw accelerations in the body frame, rad/s^2
S	Wing area, m^2
t	Time, s
$\underline{u}$	Input vector
V	Velocity, m/s
$\underline{x}$	State vector
β	Sideslip angle, rad
δ	Control surface deflection, rad
ϕ, θ	Roll and pitch angles in vehicle-carried Earth frame, rad

*Master Student.
†Assistant professor, e.vankampen@tudelft.nl, AIAA Member.
‡Associate professor, q.p.chu@tudelft.nl, AIAA Member.

ν	Virtual control input
ρ	Air density, kg/m^3
Subscript	
a, e, r	Aileron, Elevator, Rudder

I. Introduction

Aeronautics has experienced many revolutionizing inventions and enhancements over the past century. One of these flight performance enhancing factors is the invention of control systems for aircraft. Automatic flight control systems are used to increase the safety of flight by reducing pilot workload and preventing potential human errors. In the period between 1993 and 2007, fatal accidents in civil aviation due to loss of control made up 15.7% of all fatal accidents, leading up to 4088 casualties worldwide.[1] In order to decrease the number of casualties, research focuses on flight control systems that are robust and fault-tolerant.

The design of flight control systems requires a lot of resources and detailed knowledge of the aerodynamics of the aircraft. Until recent decades the most common strategy for successful flight control was based on the divide-and-conquer approach.[2] By linearizing the aircraft model for multiple flight conditions the required PID control gains for each condition were calculated and tuned. This method, called gain scheduling, is time-consuming, iterative and needs to be developed for each type of aircraft separately. In order to reduce the consumption of resources there is a need for a more generic approach to flight control system design.[3]

Advances in control systems engineering enabled the design of controllers for nonlinear systems. One of these nonlinear control techniques is known as feedback linearization. This methodology dates back to research of[4] and.[5] The theory behind feedback linearization is described in great detail by.[6–8] Feedback linearization showed to be promising for flight control, because it allows a nonlinear system to be controlled using linear control techniques. Feedback linearization uses a high-fidelity aerodynamic model of the aircraft to cancel the nonlinearities using state feedback and transformation.[9] Within the field of flight control, feedback linearization is often referred to as Nonlinear Dynamic Inversion (NDI).

One of the earlier papers of feedback linearization applied on aircraft describes the application of NDI on an F-18 HARV.[2] Since then, it has been applied on a variety of aircraft, including the X-35.[10] The strength of NDI lies in the fact that it can be applied in a similar fashion for different types of aircraft with a similar configuration. If the aerodynamic model is known, the method of deriving a control law is easily adapted for a new aircraft type. However, the performance of NDI-controllers suffers when inaccurate aerodynamic models are used.[11] Several approaches to deal with the sensitivity of NDI to model inaccuracies exist. One approach is to use system identification methods to update the model and thereby reduce the model inaccuracies. Another approach is the use of robust control techniques (e.g. H_∞) to find the correct control gains.[12–14] Finally, this sensitivity to model inaccuracies can be dealt with by reducing model dependency with a method known as Incremental Nonlinear Dynamic Inversion (INDI).

The concept of INDI is based on calculating the required incremental change in control input to steer the aircraft to the desired state. This is achieved by feeding back angular accelerations. INDI is a control strategy that is derived from research on NDI[15] and initially became known as Improved NDI or Modified NDI. As most aircraft are not equipped with an angular accelerometer (AA), the method relied on deriving angular accelerations from angular rate measurements. Later research suggested direct sensing of the angular accelerations, resulting in the name sensor-based NDI.[16] Nowadays this improved version of NDI is most widely known as INDI. The control law is based on the assumption that for small increments of time, a system's response to control inputs is larger than its response to changing states. This assumption allows the required increment in control input to be calculated from the system's input-dependent dynamics only, disregarding a system's state-dependent dynamics. In practice, INDI has been tested on the VAAC Harrier[17] and on a quadrotor Micro Aerial Vehicle (MAV).[18]

One of the main challenges in INDI control is the influence of signal delays on the performance of the controller. During practical testing, when perfect sensors can no longer be assumed, the transport delay introduced by the sensors can significantly reduce tracking performance.[3] Differentiating angular rates to calculate angular accelerations introduces further delay to the feedback loop. In addition, differentiating angular rate measurements can amplify sensor noise. Angular rates can be filtered to prevent noise amplification, at the cost of introducing further delay. One method to deal with these delays relies on predictive filtering.[3] Another approach is based on synchronizing time delays by applying the same filter that is applied

to the angular rate measurements to the control surface deflection measurements.[18] This paper investigates if INDI performance can be improved by directly sensing angular accelerations. Although the use of AAs was proposed,[16] no research has been conducted on the actual implementation of AA-based INDI.

The main contributions of this paper is a study on the effects of adding angular accelerometers to an INDI control loop, the effects of uncalibrated control surface feedback and the effect of sensor misalignment on the performance of INDI-based controllers. These effects are studied for the current sensor package configuration of the PH-LAB. In addition, the sensitivity of the CINDI controller to sensor delay is investigated in order to establish the tolerable sensor characteristics for a future sensor package upgrade. The controller is developed for a high-fidelity simulation model of the Cessna Citation research aircraft *PH-LAB*, co-owned by Delft University of Technology. Previous research on INDI for the PH-LAB utilized a discrete version of INDI called DINDI.[19] The control law of DINDI does not require direct feedback of angular accelerations, whereas the traditional formulation of CINDI does require angular acceleration feedback. Van 't Veld's research has shown the importance of time delay synchronization and Pseudo-Control Hedging (PCH) in order to improve INDI robustness. The next step in

The outline of this paper is as follows. Section II gives a brief introduction to the topic of INDI. Section III describes the model and sensor configuration of the PH-LAB. A detailed description of the proposed AA sensor is given in Section IV. The derivation of the proposed attitude controller is presented in Section V. Simulation results are presented in Section VI.

II. Incremental Nonlinear Dynamic Inversion

The theory behind INDI control is explained by starting with a general nonlinear system defined by Eq. 1, with state vector $\underline{x} \in \mathbb{R}^n$, control input vector $\underline{u} \in \mathbb{R}^m$ and a smooth vector field $\underline{f} \in \mathbb{R}^n$.

$$\dot{\underline{x}} = \underline{f}(\underline{x}, \underline{u}) \tag{1}$$

The output of this system is considered to be the full state vector, i.e. $\underline{y} = \underline{x}$. Analogous to the principles of NDI, a direct relation between input and output need to be found through differentiating the output equation. Since the output vector equals the state vector, differentiating the output results in the original system definition, i.e. Eq. 1. This result is approximated using a Taylor series expansion for $\underline{x}$ and $\underline{u}$ in the neighborhood of $[\underline{x}_0, \underline{u}_0]$, as demonstrated in Eq. 2, where only the first-order terms of the expansion are considered.[20] For the sake of simplification, the notations $F(\underline{x}_0, \underline{u}_0)$ and $G(\underline{x}_0, \underline{u}_0)$ are introduced to represent partial derivatives $\frac{\partial \underline{f}(\underline{x},\underline{u})}{\partial \underline{x}}$ and $\frac{\partial \underline{f}(\underline{x},\underline{u})}{\partial \underline{u}}$ respectively, observed at $\underline{x} = \underline{x}_0$ and $\underline{u} = \underline{u}_0$. Here, the subscript 0 in $\underline{x}_0$ and $\underline{u}_0$ indicates an incremental instance in time before $\underline{x}$ and $\underline{u}$.[3]

$$\begin{aligned} \dot{\underline{y}} = \dot{\underline{x}} = \underline{f}(\underline{x}, \underline{u}) &\approx \underline{f}(\underline{x}_0, \underline{u}_0) + \frac{\partial \underline{f}(\underline{x}, \underline{u})}{\partial \underline{x}}\Big|_{\substack{\underline{x}=\underline{x}_0 \\ \underline{u}=\underline{u}_0}} (\underline{x} - \underline{x}_0) + \frac{\partial \underline{f}(\underline{x}, \underline{u})}{\partial \underline{u}}\Big|_{\substack{\underline{x}=\underline{x}_0 \\ \underline{u}=\underline{u}_0}} (\underline{u} - \underline{u}_0) \\ &\approx \dot{\underline{x}}_0 + F(\underline{x}_0, \underline{u}_0)\,(\underline{x} - \underline{x}_0) + G(\underline{x}_0, \underline{u}_0)\,(\underline{u} - \underline{u}_0) \end{aligned} \tag{2}$$

The approximation resulting from Eq. 2 can be simplified by assuming that during an incremental instance in time a system's response to control inputs is significantly larger than a system's response to its states. This assumption is also known as the principle of time scale separation.[3] For the case of rotational aircraft dynamics, this principle implies that during a small increment in time an aircraft will shows larger responses to control surface deflections than to changing aircraft states, i.e. $F(\underline{x}_0, \underline{u}_0)\,(\underline{x} - \underline{x}_0) << G(\underline{x}_0, \underline{u}_0)\,(\underline{u} - \underline{u}_0)$. The simplified approximation is given by Eq. 3, where $\Delta\underline{u} = (\underline{u} - \underline{u}_0)$.

$$\dot{\underline{x}} \approx \dot{\underline{x}}_0 + G(\underline{x}_0, \underline{u}_0)\Delta\underline{u} \tag{3}$$

Eq. 3 can be solved for the incremental change in control input $\Delta\underline{u}$ by defining the virtual control input as $\underline{nu} = \dot{\underline{x}}$:

$$\Delta\underline{u} = G^{-1}(\underline{x}_0, \underline{u}_0)\,[\underline{\nu} - \dot{\underline{x}}_0] \tag{4}$$

The new control input is defined as the current control input $\underline{u}_0$ plus the incremental change in control input.

$$\underline{u} = \underline{u}_0 + \Delta\underline{u} \tag{5}$$

III. Aircraft Model

The aircraft model that is used for this research is a Cessna Citation 500, a CS-25 fixed-wing aircraft with two turbine engines. Roll, pitch and yaw are generated by deflecting the aileron, elevator and rudder respectively. The proposed controller utilizes two sets of reference frames, both vehicle-carried. The first reference frame is the body frame ($0x_By_Bz_B$), defined along the longitudinal, lateral and vertical axes of the airframe. The second reference frame is the vehicle-carried Earth reference frame ($0x_Ey_Ez_E$), defined in the center of gravity of the aircraft, with the axes pointing towards North, East and Down respectively.

The three-dimensional moment equilibrium is given by Eq. 6. Here, $\underline{M}$ represents the moment vector, I represents the inertia tensor, $\underline{\omega}$ represents the angular rate vector and $\underline{\dot{\omega}}$ represents the angular accelerations. Since the moment equation is considered in the aircraft's body frame, the rotation of the frame with respect to an inertial frame have to be considered. This is described by the term $\underline{\omega} \times I\underline{\omega}$.

$$\underline{M} = I\underline{\dot{\omega}} + \underline{\omega} \times I\underline{\omega} \tag{6}$$

Eq. 6 can be expanded as shown in Eq. 7. Here, L, M and N represent the rolling, pitching and yawing moments respectively. Roll, pitch and yaw rates are denoted as p, q and r respectively.

$$\underline{M} = \begin{bmatrix} L \\ M \\ N \end{bmatrix} = \begin{bmatrix} I_{xx} & 0 & -I_{xz} \\ 0 & I_{yy} & 0 \\ -I_{xz} & 0 & I_{zz} \end{bmatrix} \begin{bmatrix} \dot{p} \\ \dot{q} \\ \dot{r} \end{bmatrix} + \begin{bmatrix} p \\ q \\ r \end{bmatrix} \times \begin{bmatrix} I_{xx} & 0 & -I_{xz} \\ 0 & I_{yy} & 0 \\ -I_{xz} & 0 & I_{zz} \end{bmatrix} \begin{bmatrix} p \\ q \\ r \end{bmatrix} \tag{7}$$

The external aerodynamic moments are described by Eq. 8, where the aerodynamic moments are a function of the aerodynamic moment coefficients C_l, C_m and C_n, air density ρ airspeed V, wing area S, mean aerodynamic chord $\bar{c}$ and wing span b.

$$\underline{M} = \begin{bmatrix} L \\ M \\ N \end{bmatrix} = \begin{bmatrix} b \cdot C_l \\ \bar{c} \cdot C_m \\ b \cdot C_n \end{bmatrix} \cdot \frac{1}{2}\rho V^2 S \tag{8}$$

In Eq. 8, the aerodynamic moment coefficients C_l, C_m and C_n can be rewritten in terms of a first order Taylor series expansion, as shown in Equations 9 to 11.

$$C_l = C_{l_0} + C_{l_\beta}\beta + C_{l_p}\frac{pb}{2V} + C_{l_r}\frac{rb}{2V} + C_{l_{\delta_a}}\delta_a + C_{l_{\delta_r}}\delta_r \tag{9}$$

$$C_m = C_{m_0} + C_{m_\alpha}\alpha + C_{m_q}\frac{q\bar{c}}{V} + C_{m_{\delta_e}}\delta_e \tag{10}$$

$$C_n = C_{n_0} + C_{n_\beta}\beta + C_{n_p}\frac{pb}{2V} + C_{n_r}\frac{rb}{2V} + C_{n_{\delta_a}}\delta_a + C_{n_{\delta_r}}\delta_r \tag{11}$$

In order to distinguish the moment contribution of the control inputs from the moment contribution of the aerodynamics of the airframe, Eq. 8 is rewritten into Eq. 12, where C_{l_a}, C_{m_a} and C_{n_a} represent the combined effect of the aerodynamics of the airframe on the moment coefficients, as shown Eqs. 13 to 15. The control surface deflections $\delta_a, \delta_e, \delta_r$ represent the aileron, elevator and rudder deflections respectively.

$$\begin{bmatrix} L \\ M \\ N \end{bmatrix} = \frac{1}{2}\rho V^2 S \left\{ \begin{bmatrix} bC_{l_{\delta_a}} & 0 & bC_{l_{\delta_r}} \\ 0 & \bar{c}C_{m_{\delta_e}} & 0 \\ bC_{n_{\delta_a}} & 0 & bC_{n_{\delta_r}} \end{bmatrix} \begin{bmatrix} \delta_a \\ \delta_e \\ \delta_r \end{bmatrix} + \begin{bmatrix} bC_{l_a} \\ cC_{m_a} \\ bC_{n_a} \end{bmatrix} \right\} \tag{12}$$

$$C_{l_a} = C_{l_0} + C_{l_\beta}\beta + C_{l_p}\frac{pb}{2V} + C_{l_r}\frac{rb}{2V} \tag{13}$$

$$C_{m_a} = C_{m_0} + C_{m_\alpha}\alpha + C_{m_q}\frac{q\bar{c}}{V} \tag{14}$$

$$C_{n_a} = C_{n_0} + C_{n_\beta}\beta + C_{n_p}\frac{pb}{2V} + C_{n_r}\frac{rb}{2V} \tag{15}$$

Both Eq. 7 and 12 are equated in Eq. 16 to obtain a relation between control input and aircraft dynamics.

$$\underline{M} = I\dot{\underline{\omega}} + \underline{\omega} \times I\underline{\omega} = \frac{1}{2}\rho V^2 S \left\{ \begin{bmatrix} bC_{l_{\delta_a}} & 0 & bC_{l_{\delta_r}} \\ 0 & \bar{c}C_{m_{\delta_e}} & 0 \\ bC_{n_{\delta_a}} & 0 & bC_{n_{\delta_r}} \end{bmatrix} \begin{bmatrix} \delta_a \\ \delta_e \\ \delta_r \end{bmatrix} + \begin{bmatrix} bC_{l_a} \\ cC_{m_a} \\ bC_{n_a} \end{bmatrix} \right\} \tag{16}$$

The moment relation given by Eq. 16 can be solved for $\dot{\underline{\omega}}$, which results in Eq. 17. It should be noted that this form of the moment equation resembles the nonlinear system description $\dot{\underline{\omega}} = \underline{f}(\underline{\omega}) + G\underline{u}$, that is affine in input.

$$\dot{\underline{\omega}} = \underbrace{I^{-1}\left\{ \frac{1}{2}\rho V^2 S \begin{bmatrix} bC_{l_a} \\ cC_{m_a} \\ bC_{n_a} \end{bmatrix} - \underline{\omega} \times I\underline{\omega} \right\}}_{f(\underline{\omega})} + \underbrace{I^{-1}\frac{1}{2}\rho V^2 S \begin{bmatrix} bC_{l_{\delta_a}} & 0 & bC_{l_{\delta_r}} \\ 0 & \bar{c}C_{m_{\delta_e}} & 0 \\ bC_{n_{\delta_a}} & 0 & bC_{n_{\delta_r}} \end{bmatrix}}_{G} \underbrace{\begin{bmatrix} \delta_a \\ \delta_e \\ \delta_r \end{bmatrix}}_{\underline{u}} \tag{17}$$

IV. Angular Accelerometer

The AA that is considered for this thesis research is a *SR-207RFR* model sensor by *Columbia Research Laboratories* and it is based on the so-called fluid rotor concept. A fluid rotor AA uses a annular channel containing a fluid that responds to angular accelerations. Applying an angular acceleration on this strapdown sensor causes the casing to rotate. The inertia of the fluid would keep the fluid static while the casing is revolving around the fluid. However, vanes inside the sensor block the fluid, causing it to displace through the annular channel. The displacement of the vanes is sensed by galvanometers that convert the rotation to a current.[21]

The available sensor for this thesis is investigated and modeled by.[22,23] Using frequency response data from calibration table measurements, several transfer functions are identified that fit the data. Multiple input frequencies and amplitudes are investigated by.[22] Figure 1 shows the dynamic response of the AA to a sinusoidal acceleration input on a calibration table, with a frequency of 1 Hz and an amplitude of 400 deg/s^2. It should be noted that the measurement of the CT acceleration contains higher noise levels than the actual AA sensor. In addition it can be observed from Figure 1 that the AA shows signs of phase lag. When sampled at a frequency of 2 kHz, the delay between the CT and AA signals varies from 24 to 31 samples, corresponding to a time delay of 12.0 to 15.5 ms.

The transfer function is based on inputs of deg/s^2 and the output signal is in volts. Using a scaling gain of $K = \frac{1}{0.23}$ rad/V the output signal can be converted from volts to rad/s^2. Eq. 18 shows a 4$^{\text{th}}$ order model with a fit of 99.02%. Note that this model contains positive zeroes, making it a non-minimum phase system.

$$H_{4th}(s) = \frac{-1.672 \cdot 10^{-4}s^4 - 0.028s^3 - 68.74s^2 + 2.164 \cdot 10^4 s + 188.7}{s^4 + 314.4s^3 + 6.589 \cdot 10^4 s^2 + 5.408 \cdot 10^6 s + 4.426 \cdot 10^4} \tag{18}$$

Eq. 19 is identified using a 5$^{\text{th}}$ order transfer function and does not contain non-minimum phase behavior. This model has a fit of 99.01%.

$$H_{5th}(s) = \frac{3.983 \cdot 10^6 s + 1.01 \cdot 10^5}{s^5 + 5004.1s^4 + 1.043 \cdot 10^5 s^3 + 1.499 \cdot 10^7 s^2 + 9.946 \cdot 10^8 s + 1.346 \cdot 10^7} \tag{19}$$

After sampling the output signal of the sensor has units of volts. The sensor has a constant conversion factor of $K = 0.23$ V/rad that can be used to express the output signal in rad/s^2.

Noise levels of the sensor are obtained from a static test. The noise variance equals $1.4703 \cdot 10^{-6}$ rad/s^2. The internal misalignment of the sensors is investigated by[23] using an AAMU configuration on the CT. Three AA sensors are mounted in a 3-axes machined mounting block. The cross-axis sensitivity of accelerations is calculated to be less than 1% for all AA sensors. This result corresponds to the expected internal misalignment specified by the manufacturer.

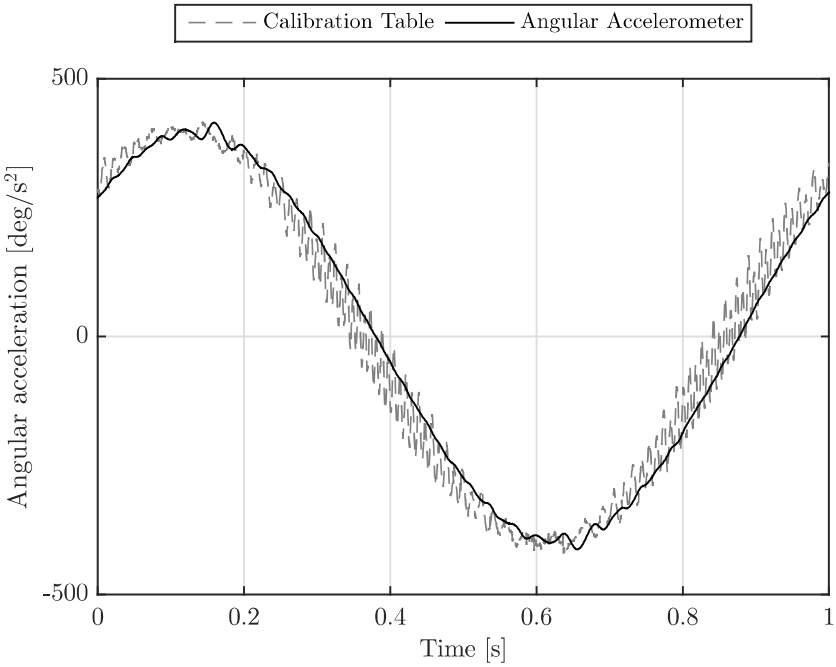

Figure 1: Angular accelerometer response to a 1 Hz input on a calibration table

V. Attitude Controller

V.A. Angular rate controller

The INDI control law is based on controlling the moments around an aircraft's principle axes. The angular accelerations of an aircraft can be controlled if moments can be generated using control effectors. This holds through the relation between angular acceleration and moments, as previously presented in Eq. 17.

$$\dot{\underline{\omega}} = \underbrace{I^{-1}\left\{\frac{1}{2}\rho V^2 S \begin{bmatrix} bC_{l_a} \\ cC_{m_a} \\ bC_{n_a} \end{bmatrix} - \underline{\omega} \times I\underline{\omega}\right\}}_{f(\underline{\omega})} + \underbrace{I^{-1}\frac{1}{2}\rho V^2 S \begin{bmatrix} bC_{l_{\delta_a}} & 0 & bC_{l_{\delta_r}} \\ 0 & \bar{c}C_{m_{\delta_e}} & 0 \\ bC_{n_{\delta_a}} & 0 & bC_{n_{\delta_r}} \end{bmatrix}}_{G} \underbrace{\begin{bmatrix} \delta_a \\ \delta_e \\ \delta_r \end{bmatrix}}_{\underline{u}} \tag{17 revisited}$$

An INDI control law can be obtained for Eq. 17. First, in Eq. 20 the dynamics are approximated using a Taylor series expansion.

$$\underline{\omega} \approx \underline{\omega}_0 + \underbrace{\frac{\partial \underline{f}}{\partial \underline{\omega}}\Big|_{\underline{\omega}=\underline{\omega}_0}}_{F(\underline{\omega}_0)} \underbrace{(\underline{\omega} - \underline{\omega}_0)}_{\Delta\underline{\omega}_0} + G\underbrace{(\underline{u} - \underline{u}_0)}_{\Delta\underline{u}} \tag{20}$$

Then using the principle of time-scale separation, it is assumed that $F(\omega)\Delta\underline{\omega} >> G\Delta\underline{u}$ and Eq. 20 simplifies to Eq. 21. The INDI control law is shown in Eq. 22.

$$\underline{\omega} \approx \underline{\omega}_0 + G\underbrace{(\underline{u} - \underline{u}_0)}_{\Delta\underline{u}} \tag{21}$$

$$\begin{aligned} &\Delta\underline{u} = G^{-1}\left(\underline{\nu} - \underline{\omega}_0\right) \text{ with:} \\ &\underline{\nu} = \dot{\underline{\omega}} \end{aligned} \tag{22}$$

Figure 2 shows the inner loop of the controller based on INDI.

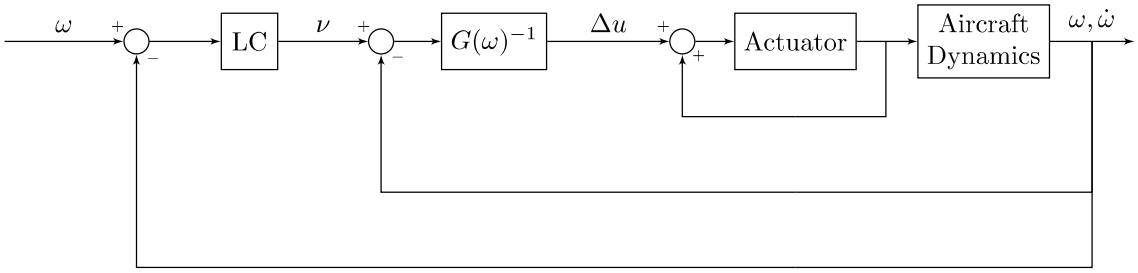

Figure 2: INDI control loop with actuator dynamics

V.B. Attitude Controller

The angular rates of the aircraft can be controlled using INDI. This rate control forms the inner loop of the automatic flight control system and is useful for pilot-in-the-loop control. When an attitude hold mode, a glide slope following mode or a navigational mode are required, the flight control system requires an outer loop that controls the attitude angels of the aircraft. This section is elaborates the control law that is used for establishing attitude control.

The aircraft's angular rates are defined in the body-frame by p, q and r. The attitude angles however are defined in a vehicle-carried Earth frame, by roll angle ϕ, pitch angle θ and yaw angle ψ. The rate of change of the attitude angles is related to the angular rates around the body axes by Eq. 23. This relation shows how the rate of change of the roll, pitch and yaw angles can be calculated in the Earth-frame using the measured rates in the body frame.

$$\begin{bmatrix} \dot{\phi} \\ \dot{\theta} \\ \dot{\psi} \end{bmatrix} = \begin{bmatrix} 1 & \sin\phi\tan\theta & \cos\phi\tan\theta \\ 0 & \cos\phi & -\sin\phi \\ 0 & \sin\phi/\cos\theta & \cos\phi/\cos\theta \end{bmatrix} \begin{bmatrix} p \\ q \\ r \end{bmatrix} \tag{23}$$

By solving Eq. 23 for p, q and r Eq. 24 is obtained. With this relation the desired rotational rates can be calculated from the rate of change of the attitude angles.

$$\begin{bmatrix} p \\ q \\ r \end{bmatrix} = \begin{bmatrix} 1 & 0 & -\sin\theta \\ 0 & \cos\phi & \sin\phi\cos\theta \\ 0 & -\sin\phi & \cos\phi\cos\theta \end{bmatrix} \begin{bmatrix} \dot{\phi} \\ \dot{\theta} \\ \dot{\psi} \end{bmatrix} \tag{24}$$

The NDI control law given by Eq. 24 is not optimal for asymmetric flight, as it does not take into account sideslip angles. In order to perform coordinated turns without lateral accelerations, not the heading angle ψ but the sideslip angle β has to be minimized. A sideslip vane is a sensor that can provide this data. Unfortunately, this sensor is not always equipped on the PH-LAB, as it is part of an optional nose boom that can sense sideslip and angle of attack. In order to increase the practical value of this controller, an alternative is required. Sideslip angles can be estimated using linear accelerometer data and body velocities u, v, w. The PH-LAB is not equipped with fast and reliable body velocity sensors.[19] Therefore, an alternative method is used based on the attitude controller designed by Van 't Veld.[19] A desired yaw rate is calculated from the lateral load factor n_y, based on the control law given in Eq. 25.

$$r_d = \frac{g}{V}(n_y + \sin\phi\cos\theta) \tag{25}$$

By rewriting the NDI control law as a function of r_d instead of $\dot{\phi}$, an approximate sideslip compensation can be incorporated. When rewriting the transformation into a form that is independent of the rate of change of the heading angle $\dot{\psi}$, the equations for roll rate p and pitch rate q have to be rewritten. This results in the outer loop control law shown in Eq. 26, where the outer loop controls the roll and pitch angles directly. The heading angle is indirectly controlled through the roll angle. Sideslip is minimized by closed-loop control of the lateral acceleration.

$$\begin{bmatrix} p \\ q \end{bmatrix} = \begin{bmatrix} 1 & \sin\phi\tan\theta \\ 0 & \cos\phi \end{bmatrix}^{-1} \left\{ \begin{bmatrix} \nu_\phi \\ \nu_\theta \end{bmatrix} - \begin{bmatrix} \frac{\tan\theta}{\cos\phi} \\ -\tan\phi \end{bmatrix} r \right\} \tag{26}$$

V.C. Pseudo Control Hedging

The actuators of the PH-LAB have physical limits in both maximum deflection and rate. These limits violate the assumption of instantaneous actuators in the theory of INDI. This essentially means that the control effectiveness is not the same for the entire deflection range of the actuator. At the saturation limits of the actuator, the maximum attainable control effort cannot increase any further. For this reason, the performance of INDI controllers degrades when the actuators reach their physical limits. Based on the works of Lombaerts, Simplicio and Van 't Veld[19,24,25] the use of Pseudo Control Hedging to mitigate performance degradation due to control surface saturation is proposed. PCH essentially reduces the command signal in order to avoid reaching saturation limits. Adding PCH to the flight controller effectively acts as a measure against integrator windup.[24]

PCH utilizes a first-order reference model (RM) to adjust the commanded rotational rate $\underline{\omega}_c$ to an achievable command $\underline{\omega}_{rm}$ using a linear gain K_{rm}, Eq. 27.

$$\underline{\nu}_{rm} = K_{rm}(\underline{\omega}_c - \underline{\omega}_r m) \tag{27}$$

The rate command is adjusted using a command hedge $\underline{\nu}_h$, Eq. 28. For non-saturated control surfaces, the control hedge $\underline{\nu}_h$ is zero.[25]

$$\underline{\omega}_{rm} = \frac{1}{2}(\underline{\nu}_{rm} - \underline{\nu}_h) \tag{28}$$

If the control surface is saturated, the command hedge is calculated with the control effectiveness G and the excess demand $u_c - u$, as shown in Eq. 29.

$$\underline{\nu}_h = G(u_c - u) \tag{29}$$

V.D. Controller overview

Table 1 shows the gain values that are used for the flight controller. The gains are kept equal to the DINDI control gains[19] to allow direct comparability between both controllers.

Table 1: INDI control gains[19]

Channel	INDI			
	Inner			Outer
	$K_{P_{in}}$	$K_{P_{rm}}$	$K_{I_{rm}}$	$K_{P_{out}}$
Roll, p-ϕ	20	7	1.4	1.5
Pitch, q-θ	20	6	1.2	1.5
Yaw, r-n_y	20	7	1.4	n.a.

Figure 3 shows the complete control diagram, including sensors and PCH.

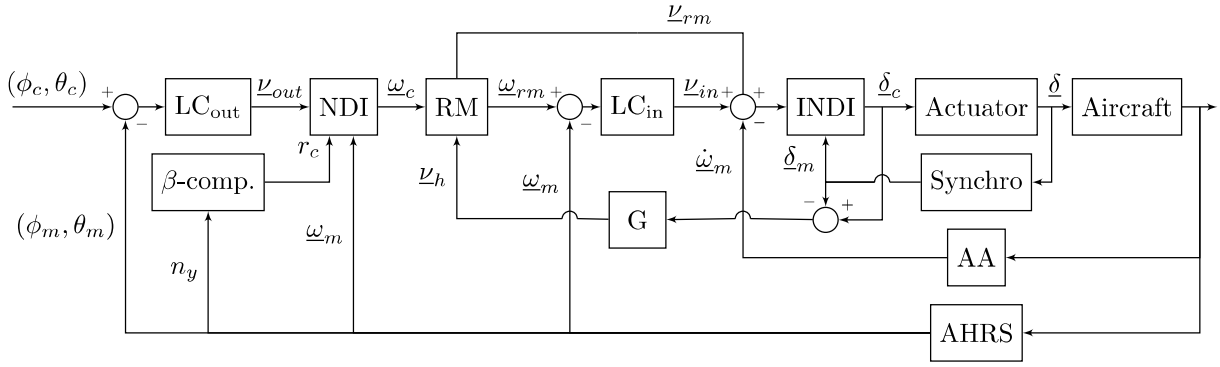

Figure 3: Complete control diagram including INDI rate control, NDI attitude control and PCH

VI. Effects of Real World Phenomena on INDI Controller Performance

Real world phenomena such as turbulence and sensor characteristics influence the performance of INDI-based flight controllers. This section describes the effects of sensor noise and bias, transport delays and unsynchronized sampling frequencies on the performance of the developed FCS. The experiment uses a high-fidelity model to simulate 40 seconds of flight during which consecutively four 3211 maneuvers are flown. The commands alternate from a ±10 degrees pitch angle command to a ±10 degrees roll angle command. This simulation set-up are based on the experiments of Van 't Veld,[19] allowing direct comparability of the two sensor configurations. As a controller performance assessment metric the RMS value of the combined tracking error of the outer loop control variables (ϕ, θ, β) is used.[19] Roll and pitch angles are used for maneuvering, whereas the sideslip angle is steered to zero to assure coordinated turns. The experiment is performed at an altitude of 6000 m at an airspeed of 100 m/s.

VI.A. Overview of Real-World Phenomena

The real-world phenomena that are considered for this paper are mostly based on the research of van 't Veld.[19] Two types of phenomena are considered, namely signal characteristics and atmospheric turbulence. The signal characteristics of the current sensor package are listed in Table 2,[19] with the addition of the AA signal characteristics.[22] Atmospheric turbulence is modeled with the Dryden model, with $\sigma = 1\text{m}^2/\text{s}^2$ and $L_g = 150$ m.[19] Lastly, a constant wind bias of 25 m/s is divided over the three body axes and included in the experiments.[19]

Table 2: PH-LAB Cessna Citation sensor signal characteristics, adapted from[19]

	Bias [μ]	Noise [σ^2]	Delay [s]	Sampling Time [s]
p, q, r [rad/s]	$3 \cdot 10^{-5}$	$4 \cdot 10^{-7}$	0.128	0.0192
V [m/s]	2.5	$8.5 \cdot 10^{-4}$	0.1	0.0625
$\delta_a, \delta_e, \delta_r$ [rad]	$4.5 \cdot 10^{-3}$	$5.5 \cdot 10^{-7}$	0.0397	0.01
ϕ, θ	$4 \cdot 10^{-3}$	$1 \cdot 10^{-9}$	0.128	0.0192
n_y	$2.5 \cdot 10^{-3}$	$1.5 \cdot 10^{-5}$	0.128	0.0192
$\dot{p}, \dot{q}, \dot{r}$ [rad/s^2]	$7 \cdot 10^{-14}$	$1.5 \cdot 10^{-6}$	0.0155	0.01

This paper considers uncalibrated sensors as an additional real-world phenomenon. During a calibration test of the control surfaces it was found that the synchro measurements contain a high deviation from the true deflection. INDI control calculates the new control surface deflection using the incremental deflection plus the previous deflection. Accurate deflection angles are required for optimal performance of the INDI controller.

Figure 4 shows the calibration test data for the right and left aileron, the elevator and the rudder. The PH-LAB is equipped with one aileron deflection synchro on the starboard aileron. Since the PH-LAB has differential aileron deflection, the calibration curve can be used to determine the individual deflections of the port and starboard ailerons from the measurement signal. It can be observed from Figure 4c that the measured elevator deflection deviates significantly from the actual elevator deflection, particularly at the limits and the slope. The deviation in deflection angle is caused by the linkage between the synchro and the elevator hinge.

The results of the calibration test are used to obtain calibration curves for the aircraft sensors. These calibration curves are inverted for the purpose of modeling uncalibrated deflection sensors for the simulation model. Eqs. 30 to 33 present the identified polynomials that are used to simulate uncalibrated control surfaces. Eq. 32 confirms that the uncalibrated elevator synchro contains a significant gradient term, as expected from the results shown in Figure 4c.

$$\delta_{a_{m_r}} = 0.9798 \cdot \delta_{a_r} - 0.0627 \tag{30}$$

$$\delta_{a_{m_l}} = -0.0101 \cdot \delta_{a_l}^2 - 0.9798 \cdot \delta_{a_l} + 0.0508 \tag{31}$$

$$\delta_{e_m} = 1.2750 \cdot \delta_e + 0.1226 \tag{32}$$

$$\delta_{r_m} = 0.9664 \cdot \delta_r - 0.0299 \tag{33}$$

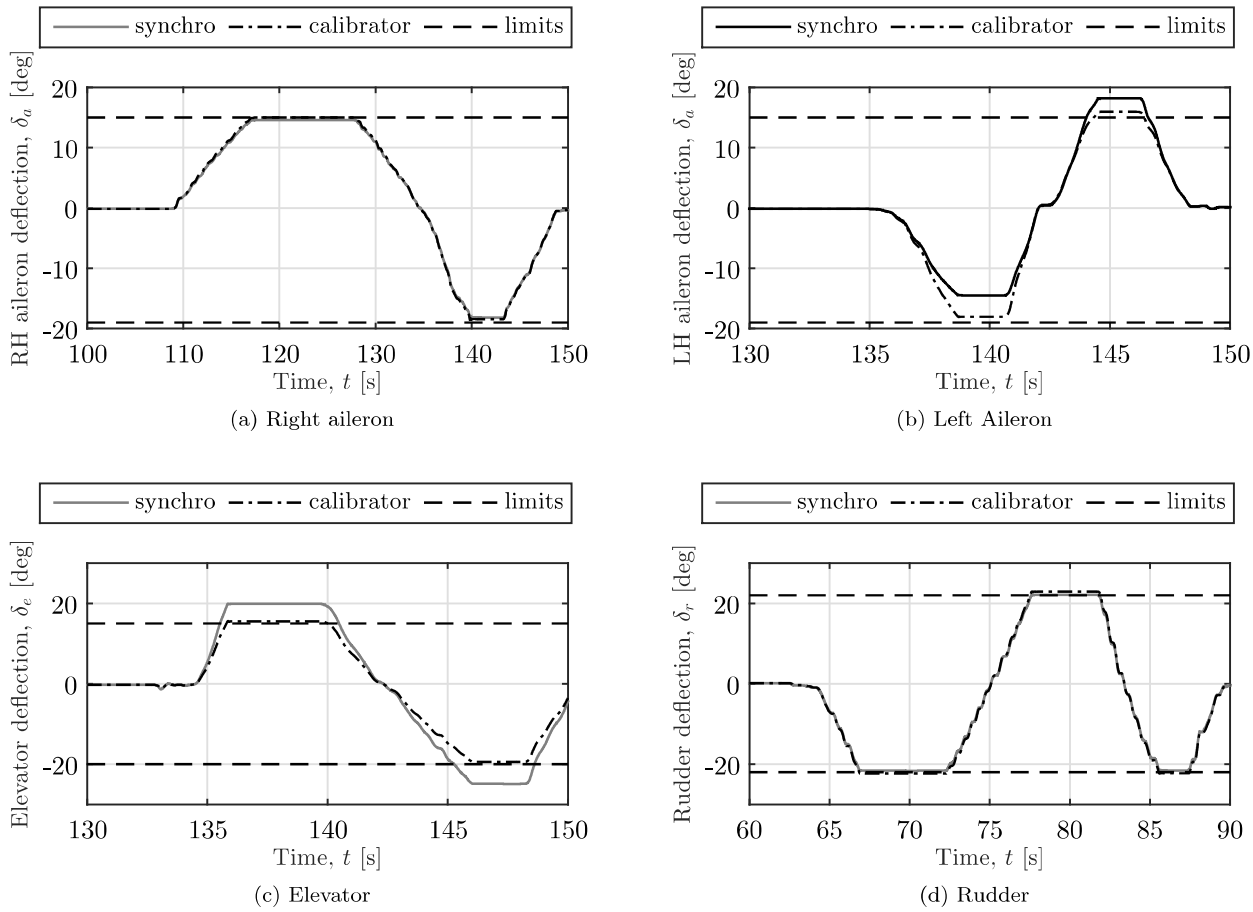

(a) Right aileron

(b) Left Aileron

(c) Elevator

(d) Rudder

Figure 4: Control surface calibration test results

Furthermore, this paper considers AA misalignment effects. The AA sensors are planned to be installed into a sensor rack. This aftermarket installation can introduce sensor misalignment.

VI.B. Results

The current sensor configuration of the PH-LAB, as discussed in Section III, adds large delays to the sensed states. Particularly the AHRS signals are significantly delayed.

Table 3 shows the effect of real world phenomena on the INDI controller performance, expressed as RMS values of the tracking error. Similarly, Table 4 shows the RMS values for the INDI controller with solutions. A solution to prevent performance degradation due to time delay issues is to synchronize time delays. Another solution is the addition of PCH to the controller. When focusing on the inner loop of the FCS, which consists of INDI rate control, the feedback signals are control surface deflection, angular rate and angular acceleration. The largest delays come from the AHRS, which supplies the angular rate feedback. By synchronizing the synchro and the AAMU to the delay level of the AHRS, all signals in the control loop are synchronized. As the research of van 't Veld indicated, the addition of constant wind bias during a 3211 maneuver significantly degrades controller performance to a level above RMS= 0.2.[19] Moreover, if delays are not synchronized, the effect of combined real-world phenomena results in a RMS value of 0.4800 when using AA sensors. As a reference, DINDI control without AA sensors has a performance of RMS= 0.2604.[19] When using AA sensors with a delay of 15.5ms, in combination with an AHRS with a delay of 128ms, the relative delay becomes too large for the controller to function properly. It can be concluded from the results of Table 3 and Table 4 that delay synchronization is necessary, especially when the relative delay between angular rates and angular accelerations is significant.

Table 3: RMS tracking error INDI

	Bias	Noise	Delay	Sampling	Baseline (100Hz)
Combined	0.26510	0.18974	0.17216	0.18795	0.1894
p, q, r	0.18936	0.18933	0.17058	0.18787	Baseline (50Hz)
V	0.18970	0.18938	0.18938	0.18934	0.18833
$\delta_a, \delta_e, \delta_r$	0.21322	0.18934	0.19204	0.18938	
ϕ, θ	0.19068	0.18937	0.19120	0.18941	Total
n_y	0.19004	0.18932	0.18945	0.18932	0.4800
$\dot{p}, \dot{q}, \dot{r}$	0.18938	0.18935	0.18919	0.18938	Total (-wind)
Wind/Turb.	0.25410	0.18982	n.a.	n.a	0.1914

Table 4: RMS tracking error INDI with delay synchronization and PCH

	Bias	Noise	Delay	Sampling	Baseline (100Hz)
Combined	0.25392	0.18891	0.17907	0.18721	0.18866
p, q, r	0.18864	0.18867	0.17852	0.18717	Baseline (50Hz)
V	0.18886	0.18866	0.18866	0.18866	0.18834
$\delta_a, \delta_e, \delta_r$	0.19057	0.18865	0.19114	0.18866	
ϕ, θ	0.19001	0.18866	0.20186	0.18869	Total
n_y	0.18935	0.18864	0.18873	0.18866	0.24041
$\dot{p}, \dot{q}, \dot{r}$	0.18866	0.18865	0.18871	0.18866	Total (-wind)
Wind/Turb.	0.25314	0.18897	n.a.	n.a.	0.18036

The time responses for the first 10 seconds of the experiment, i.e. the first 3211 pitch maneuver, are presented in Figure 5 labeled as CINDI. As a comparison, the results of the DINDI-based controller without AA feedback are shown as well.[19] It can be observed from Table 4 and from Figure 5 that the difference between both controllers is minimal, despite the significantly faster dynamics of the AA sensor. The reason for this is the fact that the inner control loop of the CINDI controller relies on the angular rate feedback to calculate the virtual control input, as can be seen in Figure 3. In the current configuration the limiting factor for better performance is formed by the AHRS.

VI.C. Controller Sensitivity to Sensor Delay

Sensor delay introduces a mismatch between the calculated control input and the sensed aircraft states. Depending on the dynamics of the aircraft and the maneuver that is performed, this mismatch can cause oscillatory behavior. As can be observed from Table 2, the largest transport delays in the proposed sensor arrangement are within the AHRS system. The AHRS system supplies both the angular rates necessary for the inner loop, as well as the attitude angles that are required for the outer loop. Another large contribution of delay can be found in the synchros that measure the deflection angle of the control surfaces. This research proposes the use of an AAMU to improve the performance of INDI control. By using an AAMU, part of the required signals can be fed back with less delay. The effect of using an AAMU on the controller performance is visualized in Figure 6. Similar to the analysis of DINDI controller performance,[19] this graph shows the RMS value of the tracking error as a function of actuator delay and angular rate delay. The results of Figure 6 concern INDI control without delay synchronization. This experiment uses a fixed delay of 15.5 ms for the AA, rather than utilizing the model described by Eq. 19. A fixed delay allows for perfect synchronization and does not concern with delay identification. An RMS value of 0.2 or lower is favorable, as oscillations occur for higher values.[19] It can be observed that the controller is more sensitive to angular rate delays then to actuator delays. Figure 6b further shows that by adding an AA, the relative delay between angular rates and accelerations decreases and therefore larger angular rate delays are tolerable.

The effect of AA delay is isolated and visualized in Figure 7. The time response of the pitch angle and elevator deflection are shown for two cases. The first case concerns the currently proposed sensor

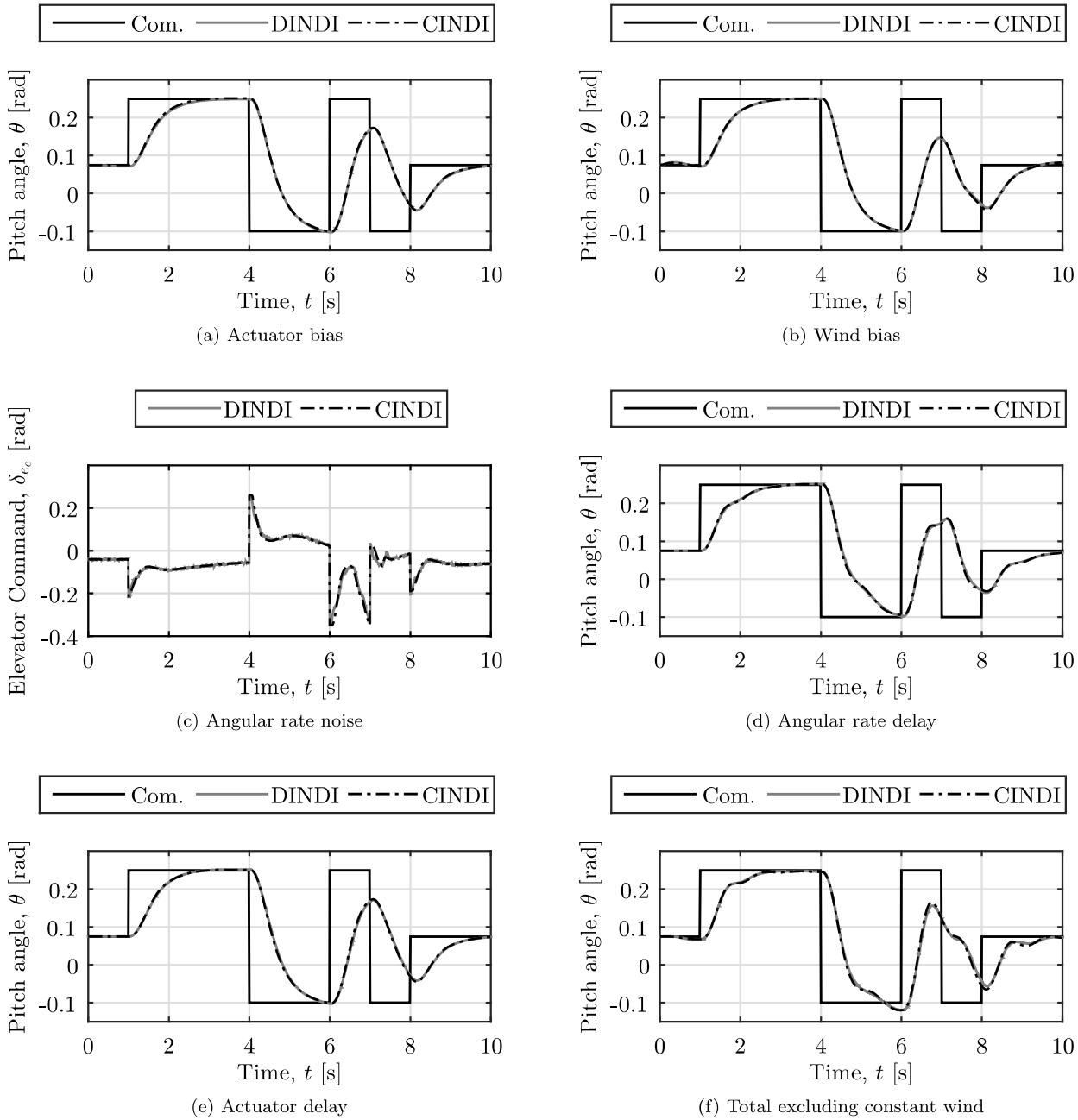

(a) Actuator bias

(b) Wind bias

(c) Angular rate noise

(d) Angular rate delay

(e) Actuator delay

(f) Total excluding constant wind

Figure 5

configuration with an AHRS and AA. The second sensor configuration concerns the AA as the only sensor with delay. It can be observed from the pitch response that the larger delay of the AHRS results in less smooth tracking behavior. Furthermore, the elevator shows larger deflections when the AHRS is included in the loop. Although the RMS value of the tracking error equals 0.17907 for *AA+AHRS*, compared to an RMS of 0.18774 for *AA*, the overall pitch response is smoother and favorable when the AHRS delays are excluded. In addition, the controller is less demanding on the control effectors without the large delays of the AHRS. The results of this experiment show the potential performance enhancements of adding AA sensors to the current sensor configuration of the PH-LAB.

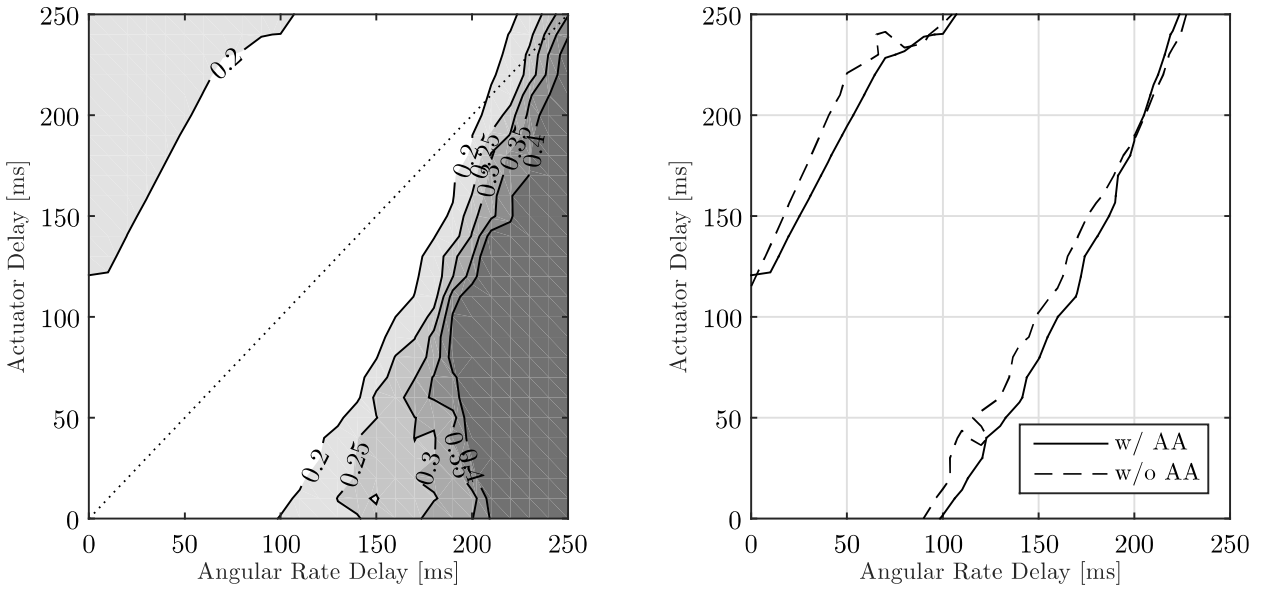

(a) RMS performance for with AA

(b) Effect of adding AA on RMS=0.2 performance boundary

Figure 6: RMS tracking error

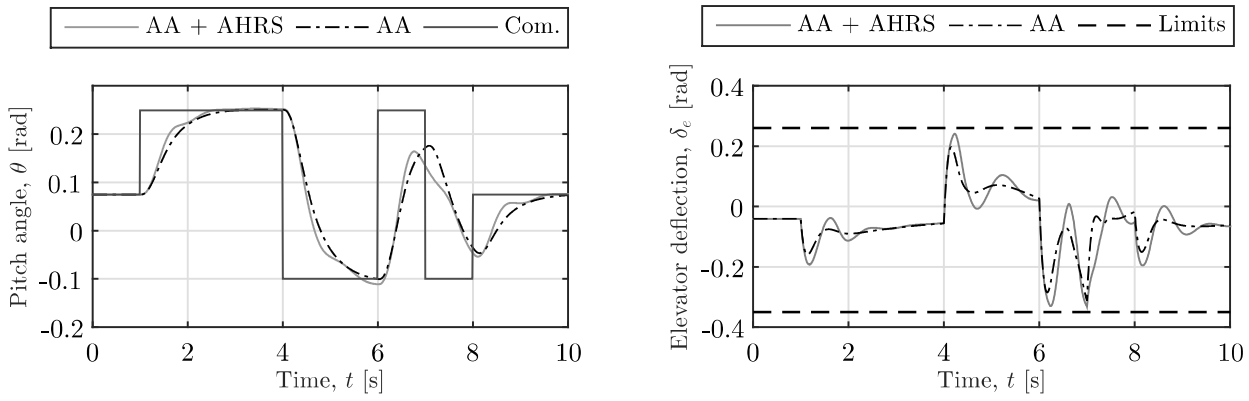

(a) Pitch angle

(b) Elevator deflection

Figure 7: Comparison of controller performance in combination with AA and AHRS sensor delays

VI.D. Influence of Uncalibrated Control Surface Deflection Measurements

The effect of uncalibrated control surface deflection measurements is simulated and visualized in Figure 8. The simulation is performed with all real-world phenomena, excluding constant wind bias. It is clear that the controller degrades more during the pitch maneuver than during the roll maneuver. This can be explained by two factors. First, the elevator deflection deviation modeled by Eq. 32 contains a large slope, resulting in a large difference between true and measured incremental deflection angles. Second, the limits of the uncalibrated elevator synchro deviate significantly from the actual physical limits. This has a large influence on controller performance since the performed maneuver demands large elevator deflections, whereas the ailerons do not reach the deflection limits. The results of this experiment underline the importance of correct deflection angle feedback for INDI controllers to perform acceptably. Furthermore it should be noted that INDI controllers can use a control surface model to supply feedback, instead of a physical sensor. In this particular sensor configuration, a control surface model could reduce the deflection signal delay from 40

ms to 10 ms (i.e. one time-step at 100 Hz).

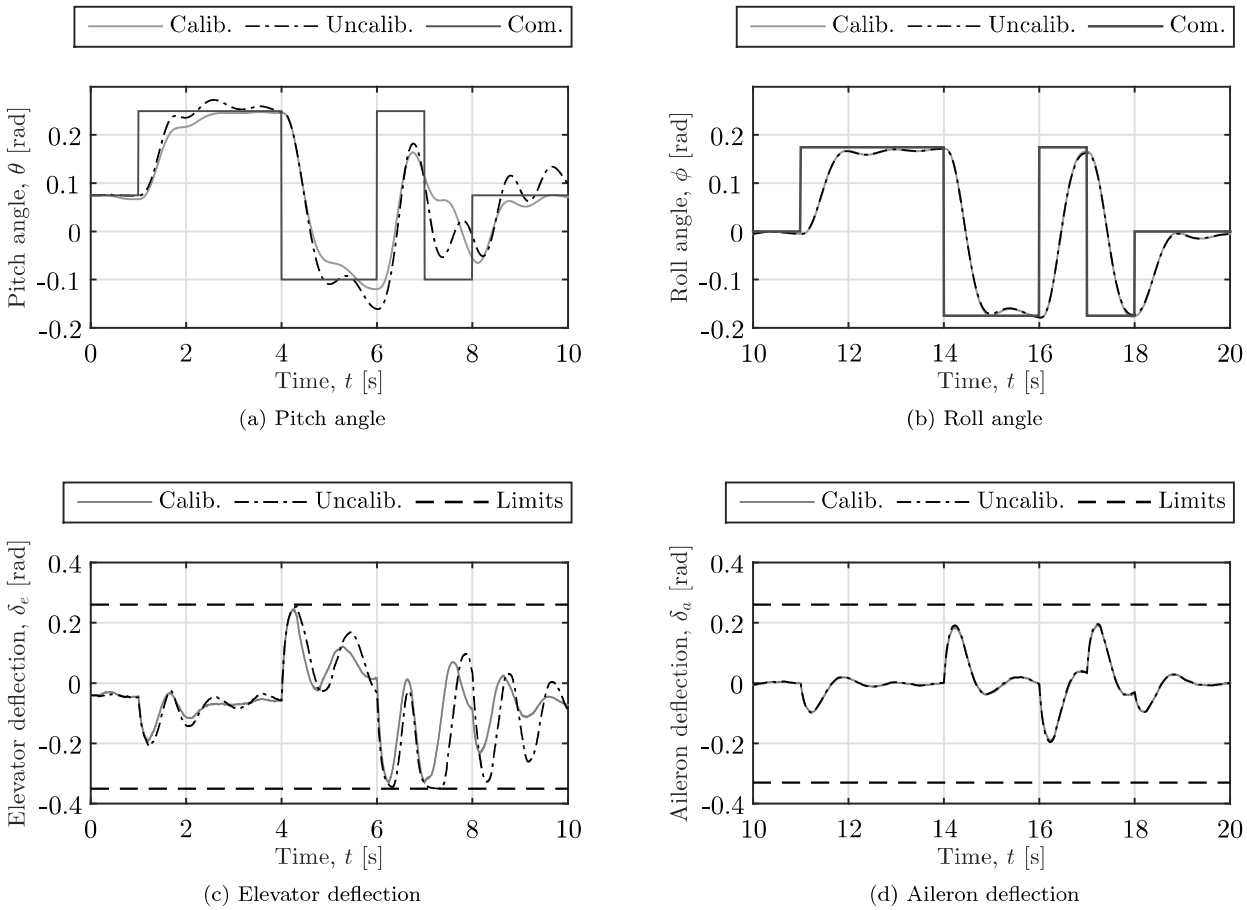

(a) Pitch angle

(b) Roll angle

(c) Elevator deflection

(d) Aileron deflection

Figure 8: Control surface calibration test results

VI.E. Influence of Angular Accelerometer Misalignment

The effects of AA misalignment on the controller performance are studied and found to be insignificant. The roll angle is hardly influenced during the 3211 pitch maneuver. The RMS value of the tracking error increases from 0.18063 to 0.18558, for a misalignment of 25 degrees. An offset of 25 degrees is not realistic in practice, but merely used to demonstrate that the impact is insignificant. It can be concluded that cross-axis sensitivity is not an issue for INDI controllers. The cross-axis coupling is rejected as any other disturbance. It should be noted that this experiment utilizes two separate channels for angular acceleration feedback and angular rate feedback, through the AA and the AHRS respectively. As INDI uses both rate and acceleration to calculate incremental changes in control input, an AA misalignment is corrected by AHRS feedback.

VI.F. Discussion of Experiment Results

The effect of real-world phenomena such as sensor noise, bias and atmospheric turbulence, on the performance of INDI-controlled aircraft have been investigated in prior research.[19] This paper presents additional experiments on INDI control applied to the same platform, with the addition of AA sensors, uncalibrated control surface deflection sensors and sensor misalignment. As the importance of PCH and time delay synchronization is analyzed and discussed by Van 't Veld,[19] the experiments of this paper do not focus on that particular aspect of INDI control. From the performed experiment with 3211 maneuvers shown in Figure 5, it can be concluded that adding an AA to the current sensor configuration does not significantly improve controller performance.

The large time delays of the angular rates supplied by the AHRS overshadow the benefits of using a fast sensor such as an AA. If the actuator and angular rate delay were to be smaller or equal to the AA delay, the benefits of the reduced time delay would be visible. It should however be noted that these benefits can be subscribed to the reduced time delay only, whether the accelerations are supplied by an AHRS-derived signal or by an AA directly. INDI control applied to the PH-LAB using the current sensor configuration can only benefit from the fast dynamics of the AA if the signals were to integrated to obtain angular rates with reduced delay. This requires sensor fusion, where the AA and AHRS are used parallel to obtain fast, accurate and reliable angular rates. In addition, to prevent the deflection synchros from adding the largest time delay to the system, it is recommended to use a deflection model rather than feedback from the synchros. The control surface calibration test indicates that the synchro measurements contained significant deviations. The difference in calibrator measurements and synchro measurements is most likely caused by the mechanical linkage between the control surface hinge points and the synchro. Mechanical wear and slack in the actuation system explain the difference between the expected deflection limits and the actual deflection limits.

Finally, a test was performed to investigate the required precision for installing the AA sensor to the aircraft. It is found that the INDI controller tolerates large sensor offsets, as the controller treats them as disturbances. The offsets are compensated by the angular rate feedback. It is recommended to investigate if an AA offset influences controller performance when the AA is used to integrate angular rates.

VII. Conclusion

Incremental nonlinear dynamic inversion (INDI) is a control technique that utilizes feedback linearization together with angular acceleration feedback. Earlier research on the topic has focused on differentiating angular rate measurements to calculate angular acceleration. As a result, actuator deflection signals have to be delayed artificially in order to synchronize all feedback signals. Using an angular accelerometer (AA) can avoid introducing additional delay to the system. This paper analyzes the effect of using angular accelerometer (AA) sensor feedback on INDI controller performance, applied on a CS-25 certified aircraft model. Using simulation experiments, the effects of adding AAs is analyzed. In addition, the effects of uncalibrated sensors is analyzed and discussed. With the current sensor configuration, the aircraft does not benefit from the addition of an AA sensor to the feedback loop. This is caused by the large transport delay of the Attitude and Heading Reference System (AHRS) that is currently installed in the aircraft. The control law of INDI utilizes both angular rate and acceleration feedback. If either one of the signals is delayed with respect to the other, both signals delays are to be synchronized to prevent performance degradation. In addition to rate and acceleration, INDI control relies on feedback of the current control surface deflection angles. Control surface deflections are supplied by synchros. The synchros in the current sensor configuration contain larger transport delays than the proposed AA sensor. From the performed experiments it can be concluded that adding an AA to the current sensor configuration does not yield significant performance enhancements. The AA sensor's fast dynamic properties cannot be fully utilized by the fact that the other sensors in the loop are significantly slower.

Furthermore, the control surface calibration experiments indicated significant deviations in the measured deflection angles. The effect of these mismatches on INDI control performance is found to be most severe when the limits of the control surface deviate and when the rate of change of the control surface deflection deviates from the actual rate of change. The results of this experiment underline the importance of accurate feedback of deflection angles.

Finally, an experiment involving AA sensor misalignment is performed, with sensor offsets of up to 25 degrees. These offsets result in cross-axis sensing of angular accelerations. Angular rate gyros compensate for this misalignment, resulting in minimal cross-axis sensitivity in closed loop. The experimental results of this paper confirm the robustness properties of INDI-based flight controllers. Time delay-induced oscillations remain a disadvantage of INDI that require synchronization of all closed-loop delay signals. Utilizing AA sensors improves INDI performance if the delay of the AA is larger or equal to the angular rate and actuator delays. If however the delay of the AA is smaller than the angular rate and actuator delays, INDI control can be improved by using sensor fusion.

References

[1]Anonymous, "Civil aviation safety data, 1993-2007," Tech. rep., Civil Aviation Authority the Netherlands, The Hague, the Netherlands, 2008.

[2]Enns, D., Bugajski, D., Hendrick, R., and Stein, G., "Dynamic inversion: an evolving methodology for flight control design," *International Journal of Control*, Vol. 59, No. 1, 1994, pp. 71–91.

[3]Sieberling, S., Chu, Q. P., and Mulder, J. A., "Robust Flight Control Using Incremental Nonlinear Dynamic Inversion and Angular Acceleration Prediction," *Journal of Guidance, Control, and Dynamics*, Vol. 33, No. 6, 2010, pp. 1732–1742.

[4]Krener, A., "A Decomposition Theory for Differentiable Systems," *SIAM Journal on Control and Optimization*, Vol. 15, No. 5, 1977, pp. 813–829.

[5]Brockett, R. W., "Feedback Invariants for Nonlinear Systems," *IFAC Congress*, International Federation of Automatic Control, Helsinki, Finland, June 1978, pp. 1150–1120.

[6]Isidori, A., *Nonlinear Control Systems*, Springer, New York City, NY, USA, 3rd ed., 1985.

[7]Nijmeijer, H. and van der Schaft, A., *Nonlinear Dynamical Control Systems*, Springer, New York City, NY, USA, 1st ed., 1990.

[8]Slotine, J. and Li, W., *Applied Nonlinear Control*, Prentice Hall Inc., Upper Saddle River, NJ, 3rd ed., 1991.

[9]Acquatella, P. B., Falkena, W., van Kampen, E.-J., and Chu, Q. P., "Robust Nonlinear Spacecraft Attitude Control Using Incremental Nonlinear Dynamic Inversion," *AIAA Guidance, Navigation, and Control Conference*, American Institute of Aeronautics and Astronautics, Minneapolis, MN, USA, August 2012, pp. 1–20.

[10]Walker, G. P. and Allen, D. A., "X-35B STOVL Flight Control Law Design and Flying Qualities," *2002 Biennial International Powered Lift Conference and Exhibit*, November 2002.

[11]da Costa, R. R., Chu, Q. P., and Mulder, J. A., "Reentry Flight Controller Design Using Nonlinear Dynamic Inversion," *Journal of Spacecraft and Rockets*, Vol. 40, No. 1, 2003.

[12]Reiner, J., Balas, G. J., and Garrard, W. L., "Flight Control Design Using Robust Dynamic Inversion and Time-scale Separation," *Automatica*, Vol. 32, No. 11, 1996, pp. 1493–1504.

[13]Juliana, S., Chu, Q. P., Mulder, J. A., and van Baten, T. J., "The Analytical Derivation of Non-linear Dynamic Inversion Control for Parametric Uncertain System," *AIAA Guidance, Navigation, and Control Conference and Exhibit*, American Institute of Aeronautics and Astronautics, San Francisco, CA, USA, 2005, pp. 1–14.

[14]Lee, H., Reiman, S., Dillon, C., and Youssef, H., "Robust Nonlinear Dynamic Inversion Control for a Hypersonic Cruise Vehicle," *AIAA Guidance, Navigation, and Control Conference and Exhibit*, American Institute of Aeronautics and Astronautics, Hilton Head, SC, USA, August 2007, pp. 1–10.

[15]Smith, P. R., "A Simplified Approach to Nonlinear Dynamic Inversion Based Flight Control," *23rd Atmospheric Flight Mechanics Conference*, American Institute of Aeronautics and Astronautics, Boston, MA, USA, 1998, pp. 762–770.

[16]Bacon, B. J. and Ostroff, A. J., "Reconfigurable Flight Control Using Nonlinear Dynamic Inversion with a Special Accelerometer Implementation," *AIAA Guidance, Navigation, and Control Conference*, American Institute of Aeronautics and Astronautics, Denver, CO, USA, August 2000, pp. 1–15.

[17]Smith, P. R. and Berry, A., "Flight Test Experience of a Non-linear Dynamic Inversion Control Law on the VAAC Harrier," *Atmospheric Flight Mechanics Conference*, American Institute of Aeronautics and Astronautics, Denver, CO, USA, 2000, pp. 132–142.

[18]Smeur, E. J. J., Chu, Q. P., and de Croon, G. C. H. E., "Adaptive Incremental Nonlinear Dynamic Inversion for Attitude Control of Micro Aerial Vehicles," *Journal of Guidance, Control, and Dynamics and Dynamics*, Vol. 39, No. 3, 2016, pp. 1–16.

[19]van 't Veld, R. C., *Incremental Nonlinear Dynamic Inversion Flight Control: Stability and Robustness Analysis and Improvements*, Master's thesis, Delft University of Technology, October 2016.

[20]Bacon, B. J., Ostroff, A. J., and Joshi, S. M., "Nonlinear Dynamic Inversion Reconfigurable Controller Utilizing a Fault Tolerant Accelerometer Approach," *Proceedings of the 19th Digital Avionics Systems Conference*, IEEE, Philadelphia, PA, USA, 2000, pp. 6F5/1 – 6F5/8.

[21]Titterton, D. H. and Weston, J., *Strapdown Inertial Navigation Technology*, The Institution of Engineering and Technology, London, UK, 2nd ed., 2005.

[22]Jatiningrum, D., de Visser, C. C., van Paassen, M. M., and Mulder, M., "Modeling an Angular Accelerometer using Frequency-Response Measurements," *AIAA Guidance, Navigation and Control Conference*, American Institute of Aeronautics and Astronautics, San Diego, CA, USA, January 2016, pp. 1–14.

[23]Jatiningrum, D., van Paassen, M., de Visser, C. C., Chu, Q. P., and Mulder, M., "Investigating Cross-Axis Sensitivity and Misalignment in an Angular Accelerometer Measurement Unit," *AIAA Guidance, Navigation, and Control Conference*, American Institute of Aeronautics and Astronautics, Grapevine, TX, USA, January 2017, pp. 1–16.

[24]Lombaerts, T. and Looye, G., "Design and Flight Testing of Nonlinear Autoflight Control Laws," *AIAA Guidance, Navigation, and Control Conference*, No. August, American Institute of Aeronautics and Astronautics, Minneapolis, MN, USA, 2012.

[25]Simplício, P., Pavel, M. D., van Kampen, E.-J., and Chu, Q. P., "An acceleration measurements-based approach for helicopter nonlinear flight control using Incremental Nonlinear Dynamic Inversion," *Control Engineering Practice*, Vol. 21, No. 8, 2013, pp. 1065–1077.